Progress In Electromagnetics Research, Vol. 138, 647–660, 2013

FAR-FIELD TUNABLE NANO-FOCUSING BASED ON METALLIC SLITS SURROUNDED WITH NONLINEAR-VARIANT WIDTHS AND LINEAR-VARIANT DEPTHS OF CIRCULAR DIELECTRIC GRATING

Peng-Fei Cao[1], Ling Cheng[1, 2], Xiao-Ping Zhang[1, *], Wei-Ping Lu[2], Wei-Jie Kong[1, 3], and Xue-Wu Liang[1, 3]

[1]School of Information Science and Engineering, Lanzhou University, Lanzhou 730000, China

[2]Department of Physics, School of Engineering and Physical Sciences, Heriot-Watt University, Edinburgh EH14 4AS, UK

[3]State Key Laboratory of Transient Optics and Photonics, Chinese Academy of Sciences, Xi'an 710119, China

Abstract—In this work, we present a new design of a tunable nanofocusing lens using a circular grating of linear-variant depths and nonlinear-variant widths. Constructive interference of cylindrical surface plasmon launched by the subwavelength metallic structure forms a subdiffraction-limited focus, the focal length can be adjusted by varying the geometry of each groove in the circular grating. According to the numerical calculation, the range of focusing points shift is much more than other plasmonic lens, and the relative phase of emitting light scattered by surface plasmon coupling circular grating can be modulated by the nonlinear-variant width and linear-variant depth. The simulation result indicates that the different relative phase of emitting light lead to variant focal length. We firstly show a unique phenomenon for the linear-variant depths and nonlinear-variant widths of the circular grating that the positive change and negative change of the depths and widths of grooves can result in different of variation trend between relative phases and focal lengths. These results paved the road for utilizing the plasmonic lens in high-density optical storage, nanolithography, superresolution optical microscopic imaging, optical trapping, and sensing.

Received 19 January 2013, Accepted 8 April 2013, Scheduled 14 April 2013

* Corresponding author: Xiao-Ping Zhang (zxp@lzu.edu.cn).

1. INTRODUCTION

The resolution of conventional optical systems is usually limited by light diffraction. This resolution limit can be overcome by using focusing evanescent waves in the near-field region. Plasmonic lens is attracting much interest recently due to its unique feature of super-resolution [1–7]. It is made up of metal and dielectric and can excite Surface Plasmon Polarisons (SPPs) [8–11]. SPP can focus the evanescent components of an illuminated object in the near-field region with subdiffraction-limit resolution [12]. This allows them to break the conventional diffraction barrier, leading to the formation of concentrated sub-wavelength light spots on the order of nanometers, so that plasmonic lens can provide super-resolution.

Researches on manipulating SPPs were so far mostly focused on specific spatial distribution of subwavelength metallic structures. Shi et al. [13] proposed a novel structure to manipulate beam, in which a metallic film is perforated with a great number of nano-slits with specifically designed widths so that the transmitted light from these slits is modulated to converge in free space. The slits transport electromagnetic energy in the form of SPPs in nanometric waveguides and provide desired phase retardations of beam manipulating with variant phase propagation constant. Further work has shown that the focusing position of plasmonic lens can be shifted by employing a group one-dimensional grating with groove depths in curved distribution [14–16]. Interestingly, it has been predicted that the relative phase at the groove exit increases steadily monotonically with the increasing groove depth, making it possible to achieve continuous phase retardation by simply designing surrounding grooves with stepped depths [17]. However, this design can only result in a maximum change of the focal position by $0.8\,\mu\text{m}$ (1.26λ), which is unable to achieve far-field nanofocusing.

Since surface plasmon polaritons is bound to a metal surface, it is an evanescent field in the vertical direction with exponential decay in amplitude and cannot reach the far field. It must take effect action to couple the SPPs into the radiating form and let higher spatial component contribute to superposition at the far-field focal region to produce subwavelength focal spot with desired dimensions. Some novel two dimensional structures can be researched, such as annular rings [18], curved chains of nanoparticles or nanoholes [19], plasmonic microzone plate (PMZP)-like or chirped slits [20, 21]. Ref. [22] took advantage of tapered dielectric grating to couple SPPs launched by two subwavelength metallic slits, therefore it can obtain the far-field focus by improving the irradiative field. Zhang et al. [23] present

a simple plasmonic lens composed of an annular slit and a single concentric groove. The subwavelength groove can scatter the SPPs and constructively interfere to get a far-field focal spot. The focal length can be adjusted by changing the groove diameter. However, the intensity at the focal spot is very weak because the scattering loss results in low focusing efficiency. In our previous work, we presented a simple method to realize far-field nanofocusing by utilizing dielectric surface grating upon the circular plasmonic lens [24]. In this scheme, a blocking chip is used to optimize the far-field plasmonic lens in order to depress the energy focusing at the incident space, and as a result the focusing efficiency is enhanced further. However, the focusing position shift also is kept within narrow limits, and reason why focal length can be modulated is not discussed.

In this paper, we present a novel method to realize far-field tunable nanofocusing by using a circular grating of linear-variant depths and nonlinear-variant widths. We find that the circular grating modulates the cylindrical surface plasmon waves, launched by annular metallic slits, so that, part of the evanescent components is coupled into the propagation waves to the far field region and to cause superfocusing effect by constructive interference. The combination of linear and nonlinear structure in the grooves plays an important role in enabling a large range of focusing position shift, between 3.3λ and 6λ. Remarkably, the reason for focusing position shift is that the relative phases at the groove exit are different. We further find that the variation trends between relative phases and focal lengths are different when the depths and widths of circular grating are different change. In $h_d > 0$ case, where h_d denotes the depth and width difference between the adjacent grooves, the rule of focusing points shift is the same as phase changing rule. On the contrary, the rule of focusing points shift has an inverse relationship to phase changing rule in $h_d < 0$ case. Our far-field tunable nanofocusing scheme can supply for the requirement of practical applications such as nanolithography, superresolution optical microscopic imaging, optical trapping, and sensing.

2. SPW DISPERSION RELATION AND WORK MODES ANALYSES

The cross section of our far-field tunable nanofocusing lens is depicted in the r-z plane, as shown in Fig. 1. The lower part is an ordinary circular plasmonic lens with several slit rings milled into metal film upon the glass substrate. Here high-intrinsic-loss metal such as titanium (Ti) or chrome (Cr) is selected, as it is benefit for the subwavelength annular slits to excite predominantly diffracted

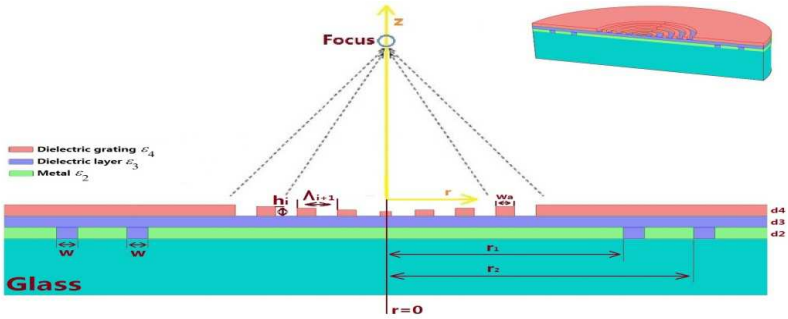

Figure 1. Schematic of the far-field nanofocusing plasmonic lens, as well as the half of the three-dimensional model is depicted at the top right corner.

cylindrical waves to launch the cylindrical surface plasmon (CSP) [20]. The multiple annular slits are milled into the metallic film; the radius and the width of each slit are denoted as r_j and w, respectively. A dielectric layer with high refractive index (n_2) is adjacent to the metal film, smoothing the metallic surface and protecting the metallic thin film from sulfuration or oxidation as well. A circular dielectric grating is finally added on the top layer, acting as a modulation device. In order to modulate the focal length, the depth (h_i) and width (Λ_i) of the circular grating can be varied. The cross-section profile of the circular grating in radial direction can be depicted in Fig. 2, where the linear-variant depth and nonlinear-variant width can be expressed as follows,

$$h_i = h_1 - h_d \times (i-1) \tag{1}$$

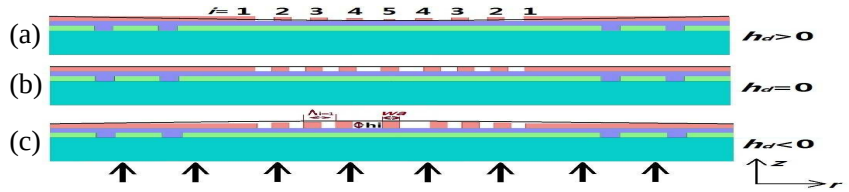

Figure 2. Schematic view of the traced linear-variant depth and nonlinear-variant width profile: w_a denotes the each groove width, Λ_i denotes the grooves width, and h_i denotes the depth of grooves with the serial number of N. h_d denotes the depth difference between the adjacent grooves, and $h_d > 0$, $h_d = 0$, $h_d < 0$ represent the cases shown in (a), (b), and (c), respectively.

$$\Lambda_i = \begin{cases} w_a + h_{\max}/2, & i = \max \text{ denote the number of the midpoint of the grating} \\ w_a + (h_{\max-1} - h_{\max}/2), & i = \max -1 \\ w_a + h_{i+1}, & i < \max -1 \end{cases} \quad (2)$$

The incident light is a radial polarization wave, impinging from the bottom of the substrate. As demonstrated in other works [25–27], the subwavelength metallic groove can scatter the SPPs into propagating waves in free space effectively according to a certain angular spectrum distribution. Utilizing this feature, a subwavelength concentric annular groove is added in the plasmonic lens, which can scatter the SPPs and constructively interfere to get a far-field focal spot [22]. Based on our previous work on the excitation and transmission of CSP waves in metal slit [24], tunable nanofocusing is formed through beam interference between the coupled SPP wave and diffraction wavelets generated from each ring of the circular grating. In a homogeneous, constant-dielectric medium, the propagation vector of the CSP waves is $k = k_0(\sigma_r \vec{r} + \sigma_z \vec{z})$, where $k_0 = 2\pi/\lambda_0$ and $\sigma_r^2 + \sigma_z^2 = \varepsilon_{metal}$. For our plasmonic structure, the E-field profile for glass layer, metal film, dielectric layer, and circular grating layer, can be given, respectively, as follows [28, 29],

$$E_r = \begin{cases} E(z)\, e^{i\left[k_0\sigma_r r \pm \sigma_{air}\left(z - d_{glass} - d_2\right)\right]} & |z| \geq d_{glass} + d_2 \\ E(z)\, e^{i[k_0\sigma_r r \pm \sigma_{air}(z - d_2)]} & d_{glass} + d_2 \leq |z| \leq d_2 \\ E(z)\, e^{i[k_0\sigma_r r \pm \sigma_{air}(z - d_3)]} & d_2 \leq |z| \leq d_3 \\ E(z)\, e^{i[k_0\sigma_r r \pm \sigma_{air}(z - d_4)]} & d_3 \leq |z| \leq d_2 \end{cases} \quad (3)$$

where d_{glass}, d_2, d_3, and d_4 are the thickness of the glass substrate, metal film, dielectric layer, and circular grating layer, respectively. The E_z and H_φ can be deduced in the same way. These electromagnetic field components are modulated by linear-variant depths and nonlinear-variant widths of the circular grating in the output surface. The final intensity at the focal point can be obtained by iteration of each zone focusing and interference each other, and can be approximately expressed as [30]

$$I = \sum_i^N \alpha_i C_i \left(\sum_j^M C_j I_{j0,i} I_{SP,j} \frac{4r_j}{\lambda_{SP}} e^{-(r_j/l_{SP})} \right) e^{-\left(\sqrt{r_i^2 + h_i^2}/\lambda_0\right)} \quad (4)$$

where λ_{SP} is the SPP wavelength as expressed in Eq. (5), λ_0 is the incident wavelength, $I_{SP,j}$ is the intensity of the SPP wave passing through the jth metal slit, l_{SP} is the propagation length for the SPP wave, α_i is interference factor of ith circular grating, $I_{i0,j}$ is the intensity of diffractive wavelet at jth slit and ith grating, h_i is height

of ith grating, r_i and r_j is the radius of each zone of grating and slits, and C_i and C_j are the coupling efficiency of the grating and slits, i and j are the number of the zones, respectively. C_i and C_j are the complicated functions of the grating and slits geometry and will likely have different functional forms when the grating and slit width are much larger or much smaller than the incident wavelength. The interference phenomena originate from both the subwavelet I_{j0} and surface plasmonic wave I_{SP}. The numerical simulation results are shown by using Finite element Method in Section 3.

$$\lambda_{sp} = \lambda_0 \sqrt{\frac{\mathrm{Re}(\varepsilon_m) + \varepsilon_d}{\mathrm{Re}(\varepsilon_m) \cdot \varepsilon_d}} \tag{5}$$

3. NUMERICAL SIMULATIONS

The softwares of COMSOL Multiphysics 4.3a and Matlab are used for simulation. We assume that the device is illuminated by a plane wave in radial polarization. A blocking chip is also used to enhancing the focusing efficiency [24]. The substrate is glass ($n_1 = 1.45$). The circular grating layer is ZnO with $n_2 = 2.16$, and the dielectric layer is artificial quartz crystal ($\varepsilon_3 = 2.4$). The metal film is selected as titanium (Ti). CSP, which is excited at metal annular slits, is closely related to the permittivity of metal [20]. The image part of metal's permittivity is associated with the intrinsic losses of metal [3]. In our lens structure, it is benefit for the subwavelength annular slits exciting diffracted cylindrical waves to launch CSP when value of metal's intrinsic-loss is higher. The Drude model [31, 32] for titanium (Ti) is taken as

$$\varepsilon_4 = \varepsilon'_{metal} + i \cdot \varepsilon''_{metal} = \left(1 - \omega_p^2 / \left(\omega^2 + i\omega\Gamma\right)\right) \tag{6}$$

where ω_p is the plasma frequency, Γ the relaxation constant, and ω the angular frequency of the source. The imaginary part of Ti is increased as the wavelength increases, as shown in Fig. 3.

The dispersion relationship in the glass-metallic-dielectric guide can be expressed in our previous work [5]. Since the polarization symmetry of a radially polarized illumination matches to the rotational symmetry cylinder structure, the entire incident beam is TM polarized with respect to the annular slit rings, enabling surface plasmon excitation from all directions. Part of the incident light is diffracted by the sharp edge of the slit, and then CSP waves are excited by the diffracted light for an extra wave vector in the direction along the film surface is obtained [33]. The glass-metallic-dielectric guide is an asymmetric structure, and there is the asymmetric surface plasmons (SPs) mode. Ref. [34] and Ref. [5] have shown that the group velocity of

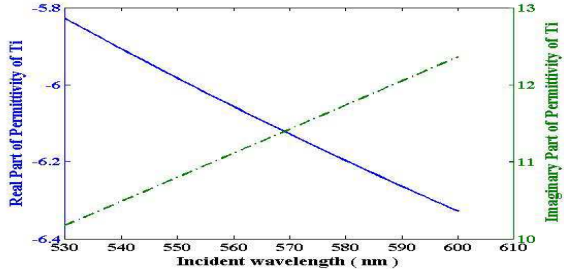

Figure 3. The relationship for permittivity of Ti.

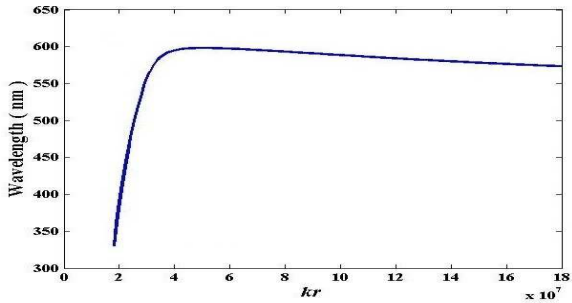

Figure 4. Dispersion curve of surface plasmons for glass-metallic-dielectric structure.

the asymmetric surface plasmons mode can be negative by engineering the dispersion curve. Because the group velocity [35] is defined as $v_g = d\omega/dk$, the slope negative at the large wave vector region when the incident wavelength is 587 nm, indicating that the group velocity is negative [34], as shown in Fig. 4. In contrast, the slope of the SPP dispersion curve is positive when the incident [5] and [34].

In order to obtain the optical energy which is transmitted into the our lens structure in this case, the reflection coefficient R on the glass-metallic-dielectric guide can be calculated by considering the resonance of the multiply reflected field [1, 5]:

$$R = \left| \frac{r_{12} + r^1 e^{(2id_1k_1)}}{1 + r_{12}r^1 e^{(2i\omega d_1 k_1)}} \right|^2 \tag{7}$$

where $k_i = \sqrt{\varepsilon_i - \varepsilon_1 \sin^2\theta_1} \times \omega/c$, $i = 1, 2, 3, 4$, $r_{ij} = (\sqrt{\varepsilon_j}\cos\theta_i - \sqrt{\varepsilon_i}\cos\theta_j)/(\sqrt{\varepsilon_j}\cos\theta_i + \sqrt{\varepsilon_i}\cos\theta_j)$, θ_i is incident angle and θ_j is the refractive angle in i layer, $r^1 = r_{23} + r^2 e^{(2id_2k_2)}/1 +$

$r_{23}r^2e^{(2id_2k_2)}$, $r^2 = r_{34} + r_{41}e^{(2id_3k_3)}/1 + r_{34}r_{41}e^{(2id_3k_3)}$. And Fig. 5 shows the reflection coefficient R as a function of the incident angle. Only incident angle is 81.36°, the value of R can be the minimum when the incident wavelength is 587 nm, which means that SPP has been excited and the most optical energy is coupled with CSP. So we choose 587 nm as incident wavelength. In order to excite the CSP effectively, the width of slits (w) should be less than half of the incident wavelength. Then the Ti slab slits are 228 nm in width, and the inner radii satisfy the principle of the destructive interference of SPPs as mentioned in Ref. [24].

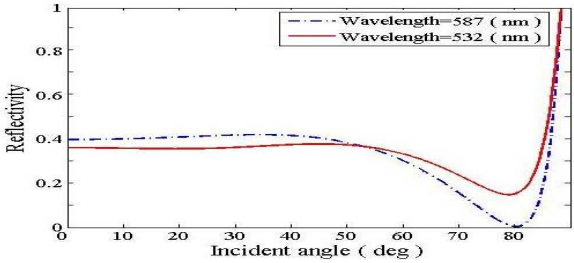

Figure 5. The reflection coefficient R as a function of the incident angle.

In following, we discuss the mechanism of focusing position shift. In order to adjust the focal length, a periodic concentric dielectric grooves is added topside, which can be treated as an annular surface grating limited by a convergent diaphragm, acting as a modulation device. The depth (h_i) and width (Λ_i) of circular grating could influence not only the coupling efficiency of the grating (C_i in Eq. (4)), but also the focusing position. The varying cross-section profile of circular grating can be expressed as Eqs. (1)∼(2), where h_d denotes the depth and width difference between the adjacent grooves. It is called the positive change (PC) of the depths and widths of circular grating when $h_d > 0$, and it is called the negative change (NC) when $h_d < 0$. Figs. 6(a)∼(c) illustrate the corresponding normalized intensity distributions for the case shown in Figs. 2(a)∼(c). Figs. 7(a)∼(c) illustrate the corresponding three-dimensional normalized intensity distributions.

The normalized intensity distribution results show that the energy emerging from the structure overlaps the axis within several microns, concentrating most of the energy in an extremely small region. For example, the $h_d = 20$ nm case shown in Fig. 6(a) reveals the focal length of 3.52 μm and the full width at half maximum (FWHM) of the

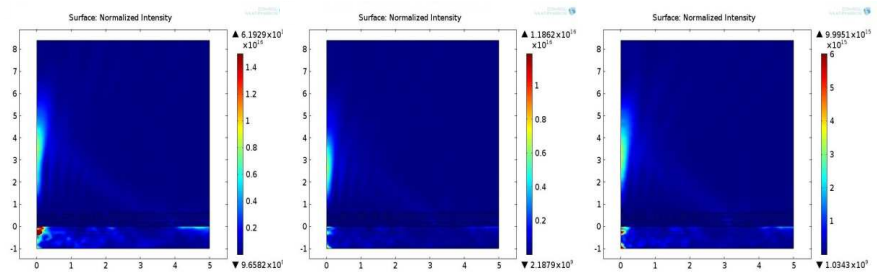

Figure 6. The normalized intensity distributions: (a) for cases shown in Fig. 2(a) with $h_d = 20\,\text{nm}$; (b) for cases shown in Fig. 2(b) with $h_d = 0\,\text{nm}$; (c) for cases shown in Fig. 2(c) with $h_d = -20\,\text{nm}$.

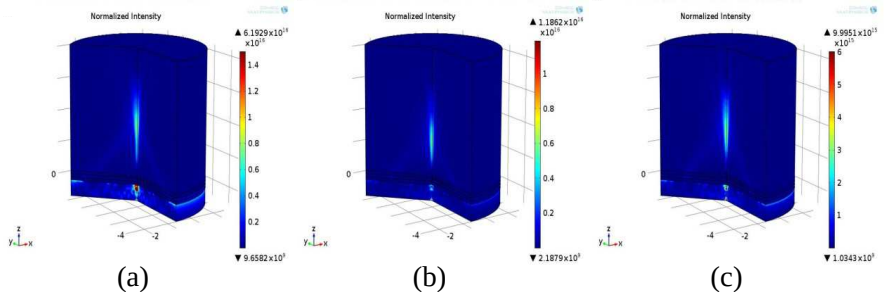

Figure 7. The three-dimensional normalized intensity distributions: (a) for cases shown in Fig. 6(a) with $h_d = 20\,\text{nm}$; (b) for cases shown in Fig. 6(b) with $h_d = 0\,\text{nm}$; (c) for cases shown in Fig. 6(c) with $h_d = -20\,\text{nm}$.

focal width of 0.35 μm, i.e., focal spot smaller than a wavelength. If $h_d = 0\,\text{nm}$, the focal length will reduce to 2.67 μm with the decreased focal width of 0.29 μm, as shown in Fig. 6(b). On the contrary, $h_d = -20\,\text{nm}$ case shows a contrary performance with the increased focal length of 3.12 μm and focal width of 0.34 μm, as shown in Fig. 6(c). Fig. 8 shows the intensity distributions of the profile of the foci.

More details of the dependence of focal length and width on groove linear-variant depth and nonlinear-variant width trace profile are shown in Fig. 9. The range of focusing points shift is about 1.94 μm (3.3λ) to 3.52 μm (6λ), which is much more than results of other lens [14–16, 22–24]. This adjusted range is much more than results as mentioned in Ref. [15] and Ref. [24]. It is worth noting that the focal length and focal width change of ups and downs by

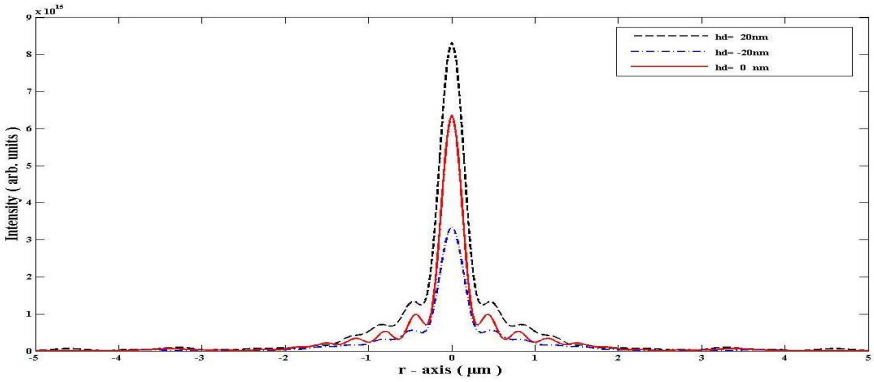

Figure 8. The intensity distributions of the profile of the foci.

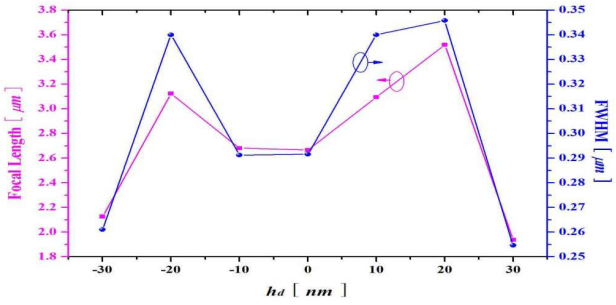

Figure 9. The focal length and focal width vary with h_d. h_d increases from -30 to 30 nm with a step of 10 nm, and the other parameters are the same as these used in Fig. 6.

increasing h_d from -30 to 30 nm at a step of 10 nm. These results are different to [15] and [24]. The reason is that the widths of circular grating are nonlinear variation, and depths are linear variation. These superimposed variation results can cause that the relative phase at the circular groove exit change of ups and downs, as shown in Fig. 10.

From Fig. 10, phase changing rules during PC and NC are different. In PC case, the rule of focusing points shift is the same as phase changing rule. On the contrary, the rule of focusing points shift has an inverse relationship to phase changing rule in NC case. Because the each depth and width of circular grating decreases or increases in PC or NC, respectively, the contributions to the phase are different. It is a unique phenomenon for the circular grating, which width is nonlinear variation, and depth is linear variation.

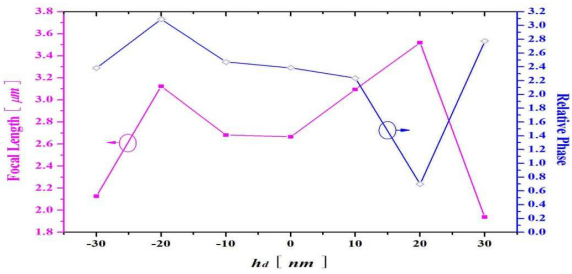

Figure 10. The focal length and relative phase vary with h_d. h_d increases from -30 to 30 nm with a step of 10 nm, and the other parameters are the same as these used in Fig. 6.

4. CONCLUSION

In this paper, we design a tunable nanofocusing lens capable of adjusting subwavelength focusing in far field under the nonlinear-variant widths and linear-variant depths of circular grating. Numerically simulations show that this adjusted range is much more than other plasmonic lens. We have revealed the relation between the linear-variant depths and nonlinear-variant widths of grooves and the relative phase of CSP in detail. Our far-field tunable nanofocusing scheme can supply for the requirement of practical applications such as nanolithography, superresolution optical microscopic imaging, optical trapping, and sensing.

ACKNOWLEDGMENT

This work was supported by National Natural Science Foundation of China (No. 61205204), "Spring sunshine" plan (No. Z2011029), the Fundamental Research Funds for the Central Universities (lzujbky-2012-42), and the Open Research Fund of State Key Laboratory of Transient Optics and Photonics, Chinese Academy of Sciences (SKLST201107).

REFERENCES

1. Pendry, J. B., "Negative refraction makes a perfect lens," *Phys. Rev. Lett.*, Vol. 85, 3966, 2000.
2. Cao, P. F., X. P. Zhang, L. Cheng, and Q. Q. Meng, "Far field imaging research based on multilayer positive- and negative-

refractive-index media under off-axis illumination," *Progress In Electromagnetics Research*, Vol. 98, 283–298, 2009.

3. Cao, P. F., L. Cheng, Y. E. Li, X. P. Zhang, Q. Q. Meng, and W. J. Kong, "Reflectivity and phase control research for superresolution enhancement via the thin films mismatch," *Progress In Electromagnetics Research*, Vol. 107, 365–378, 2010.
4. Monti, G. and L. Tarricone, "Negative group velocity in a split ring resonator-coupled microstrip line," *Progress In Electromagnetics Research*, Vol. 94, 33–47, 2009.
5. Cao, P., X. Zhang, W.-J. Kong, L. Cheng, and H. Zhang, "Superresolution enhancement for the superlens with anti-reflection and phase control coatings via surface plasmons modes of asymmetric structure," *Progress In Electromagnetics Research*, Vol. 119, 191–206, 2011.
6. Barnes, W. L., A. Dereux, and T. W. Ebbesen, "Surface plasmon subwavelength optics," *Nature*, Vol. 424, 824–830, 2003.
7. Lezec, H. J., A. Degiron, E. Devaux, R. A. Linke, F. Martín-Moreno, L. J. García-Vidal, and T. W. Ebbesen, "Beaming light from a subwavelength aperture," *Science*, Vol. 297, 820, 2002.
8. Luo, Z., T. Suyama, X. Xu, and Y. Okuno, "A grating-based plasmon biosensor with high resolution," *Progress In Electromagnetics Research*, Vol. 118, 527–539, 2011.
9. Liu, X., J. Lin, T. F. Jiang, Z. F. Zhu, Q. Q. Zhan, J. Qian, and S. He, "Surface plasmon properties of hollow AuAg alloyed triangular nanoboxes and its applications in SERS imaging and potential drug delivery," *Progress In Electromagnetics Research*, Vol. 128, 35–53, 2012.
10. Ebbesen, T. W., H. J. Lezec, H. F. Ghaemi, T. Thio, and P. A. Wolff, "Extraordinary optical transmission through sub-wavelength hole arrays," *Nature*, Vol. 391, 667–669, 1998.
11. Kumar, S., G. Sharma, and V. Singh, "Sensitivity modulation of surface plasmon resonance sensor configurations in optical fiber waveguide," *Progress In Electromagnetics Research Letters*, Vol. 37, 167–176, 2013.
12. Fang, N. and X. Zhang, "Imaging properties of a metamaterial superlens," *Appl. Phys. Lett.*, Vol. 82, 161–163, 2003.
13. Shi, H., C. Wang, C. Du, X. Luo, X. Dong, and H. Gao, "Beam manipulating by metallic nano-slits with variant widths," *Optics Express*, Vol. 13, No. 18, 6815–6820, 2005.
14. Jia, B., H. Shi, J. Li, Y. Fu, C. Du, and M. Gu, "Near-field visualization of focal depth modulation by step corrugated

plasmonic slits," *Appl. Phys. Lett.*, Vol. 94, 151912, 2009.

15. Shi, H., C. Du, and X. Luo, "Focal length modulation based on a metallic slit surrounded with grooves in curved depths," *Appl. Phys. Lett.*, Vol. 91, 093111, 2007.
16. Wang, J. and W. Zhou, "Nearfield beam shaping through tuning diffraction coupling angles," *Journal of Computational and Theoretical Nanoscience*, Vol. 7, No. 6, 1021–1024, 2010.
17. Fu, Y. and X. Zhou, "Plasmonic lenses: A review," *Plasmonics*, Vol. 5, No. 3, 287–310, 2010.
18. Liu, Z., J. M. Steele, W. Srituravanich, Y. Pikus, C. Sun, and X. Zhang, "Focusing surface plasmons with a plasmonic lens," *Nano Lett.*, Vol. 5, No. 9, 1726–1729, 2005.
19. Yin, L., V. K. Vlasko-Vlasov, J. Pearson, J. M. Hiller, J. Hua, U. Welp, D. E. Brown, and C. W. Kimball, "Subwavelength focusing and guiding of surface plasmons," *Nano Lett.*, Vol. 5, No. 7, 1399–1402, 2005.
20. Fu, Y. Q. and X. G. Luo, "Plasmonic microzone plate: Superfocusing at visible regime," *Appl. Phys. Lett.*, Vol. 91, No. 6, 061124, 2007.
21. Fu, Y., C. Du, W. Zhou, and L. E. N. Lim, "Nanopinholes-based optical superlens," *Research Letters in Physics*, Vol. 2008, 148505, 2008.
22. Zou, D. Q., "Beam adjustment with double subwavelength metal slits surrounded by tapered dielectric gratings," *Chin. Phys. Lett.* Vol. 27, No. 1, 17801, 2010.
23. Zhang, M., J. Du, H. Shi, S. Yin, L. Xia, B. Jia, M. Gu, and C. Du, "Three-dimensional nanoscale far-field focusing of radially polarized light by scattering the SPPs with an annular groove," *Optics Express*, Vol. 18, No. 14, 14664–14670, 2010.
24. Cheng, L., P. Cao, Y. Li, W. Kong, X. Zhao, and X. Zhang, "High efficient far-field nanofocusing with tunable focus under radial polarization illumination," *Plasmonics*, Vol. 7, No. 1, 175–184, 2012.
25. López-Tejeira, F., F. García-Vidal, and L. Martín-Moreno, "Scattering of surface plasmons by one-dimensional periodic nanoindented surfaces," *Phys. Rev. B*, Vol. 72, No. 16, 161405, 2005.
26. Nikitin, A., F. Lopez-Tejeira, and L. Martin-Moreno, "Scattering of surface plasmon polaritons by one dimensional in homogeneities," *Phys. Rev. B*, Vol. 75, No. 3, 35129, 2007.
27. Yu, L., D. Lin, Y. Chen, Y. Chang, K. Huang, J. Liaw, J. Yeh,

J. Liu, C. Yeh, and C. Lee, "Physical origin of directional beaming emitted from a subwavelength slit," *Phys. Rev. B*, Vol. 71, No. 4, 41405, 2005.

28. Lockyear, M. J., A. P. Hibbins, and J. R. Sambles, "Surfacetopography-induced enhanced transmission and directivity of microwave radiation through a subwavelength circular metal aperture," *Appl. Phys. Lett.*, Vol. 84, 2040–2042, 2004.
29. Fu, Y., W. Zhou, and L. E. N. Lim, "Near-field behavior of zone-plate-like plasmonic nanostructures," *JOSA A*, Vol. 25, No. 1, 238–249, 2008.
30. Fu, Y. and W. Zhou, "Hybrid Au-Ag subwavelength metallic structures with variant periods for superfocusing," *J. Nanophoton.*, Vol. 3, No. 1, 033504, 2009.
31. Fox, M., *Optical Properties of Solids*, Oxford Univerity Press, 2001.
32. Lee, K. H., I. Ahmed, R. S. M. Goh, E. H. Khoo, E. P. Li, and T. G. G. Hung, "Implementation of the FDTD method based on Lorentz-Drude dispersive model on GPU for plasmonics applications," *Progress In Electromagnetics Research*, Vol. 116, 441–456, 2011.
33. Youngworth, K. and T. Brown, "Focusing of high numerical aperture cylindrical-vector beams," *Optics Express*, Vol. 7, No. 2, 77–87, 2000.
34. Liu, Y., D. F. P. Pile, Z. Liu, D. Wu, C. Sun, and X. Zhang, "Negative group velocity of surface plasmons on thin metallic films," *Proc. SPIE*, Vol. 6323, 63231M, 2006.
35. Monti, G. and L. Tarricone, "Negative group velocity in a split ring resonator-coupled microstrip line," *Progress In Electromagnetics Research*, Vol. 94, 33–47, 2009.